CALPHAD: Computer Coupling of Phase Diagrams and Thermochemistry 52 (2016) 21–37

Contents lists available at ScienceDirect

CALPHAD: Computer Coupling of Phase Diagrams and Thermochemistry

journal homepage: www.elsevier.com/locate/calphad

Invited article

Thermodynamic assessment of the Al–Cu–Zn system, Part III: Al–Cu–Zn ternary system

Song-Mao Liang, Rainer Schmid-Fetzer*

Institute of Metallurgy, Clausthal University of Technology, d-38678 Clausthal-Zellerfeld, Germany

ARTICLE INFO

Article history:
Received 24 September 2015
Received in revised form
16 November 2015
Accepted 17 November 2015

Keywords:
Calphad assessment
Al–Cu–Zn system
Phase equilibria
Thermodynamics

ABSTRACT

A comprehensive thermodynamic reassessment of the Al–Cu–Zn system is elaborated covering the complete ternary composition range and compared with all presently available experimental phase equilibrium and thermodynamic data. One key distinction compared to previous CALPHAD work is the thermodynamic modeling of the γ phases, which is based on a detailed discussion of the crystal structure and simplified only to an extent necessary for a viable application in the ternary system. That entails significant changes in the ternary solid solution range of these phases. Revised aspects of the Al–Cu and Cu–Zn binary systems, elaborated in the reassessment in Parts I and II of this series, are incorporated as basis of the ternary system in this final Part III.

1. Introduction

The Calphad (calculation of phase diagrams) approach and more broadly the ICME (Integrated Computational Materials Engineering) framework provides powerful guidelines in design and development of new materials [1]. The thermodynamic description of Al–Cu–Zn ternary system is of great importance for developing Al alloys, Cu alloys and Zn alloys using Calphad and ICME. Currently, the work of Liang and Chang [2] is the only available full thermodynamic description of Al–Cu–Zn ternary system. Borggren and Selleby [3] revised the thermodynamic ternary interaction parameters of the liquid phase and Fcc phase from [2] in order to fit their experimental data at Cu-rich corner. Miettinen [4] provided another thermodynamic description focused on the Cu-rich corner only. However, that dataset cannot even reproduce the proper binary phase diagrams Al–Cu and Cu–Zn, not to speak of the ternary in full composition range. As we have pointed out in Part I [5] and Part II [6] of this series on the Al–Cu–Zn system, the binary sub-systems accepted in [2] contains several crucial shortages. In the present work, a thermodynamic reassessment of the Al–Cu–Zn ternary system has been carried out based on the newly reassessed binary Cu–Zn [5] and Al–Cu [6] sub-systems and providing a comprehensive comparison to all experimental data in the complete Al–Cu–Zn composition range.

2. Critical review of experimental literature data

Ghosh et al. [7] reviewed all the experimental work available on the Al–Cu–Zn ternary system up to the year of 2002. After checking with the original sources, we generally accept the experimentally assessed ternary phase diagram data provided by [7], except several key distinctions, mainly on γ phases, which will be discussed later. Therefore, most of the original references from the years 1905–2002 evaluated in [7] are not duplicated here. In the present work, the assessed phase diagrams in [7], liquidus projection and isothermal sections, have been basically accepted as experimental results for comparison to keep this work concise. More recent experimental work [3,8–14] and original data interpreted differently from [7], mainly [15–18], are considered in more detail with reference to the original work.

Data on all solid phases in the Al–Cu–Zn system are compiled in Table 1 [2,7,19–21]. Proper phase notations are crucial to avoid confusion in this complex system. For convenience the phase names used in [7] are also given and the crystal structure data to provide unique identification. The current phase notations in Table 1 are consistent with those in the binary phase diagrams of Parts I and II [5,6] and the sole phase γ in the Cu–Zn system corresponds to the phase γ_2 in the ternary.

The complete solid solution range of the "γ phase" assessed in [7] is not accepted in this work based on the examination detailed below. In all of the assessed isothermal sections from 350 °C to 700 °C in [7], the γ phase region is continuous from Al–Cu side (γ-Cu_9Al_4, cP52 structure) to Cu–Zn side (γ-Cu_5Zn_8, cI52

* Corresponding author.
E-mail addresses: songmao.liang@tu-clausthal.de (S.-M. Liang), schmid-fetzer@tu-clausthal.de (R. Schmid-Fetzer).

http://dx.doi.org/10.1016/j.calphad.2015.11.001
0364-5916/

Table 1
Solid phases in the Al–Cu–Zn system.

Phase notation, name in TDB [this work]	Sublattice model [this work]	Sublattice model [2]	Phase name[a]/temperature range (°C)[a]	Pearson symbol/*space group*/ prototype[a]
(Al), Fcc	(Al,Cu,Zn)1	(Al,Cu,Zn)1	(αAl) ≤660.452	cF4 *Fm-3m* Cu
(Cu), Fcc	(Al,Cu,Zn)1	(Al,Cu,Zn)1	(αCu) ≤1084.87	cF4 *Fm-3m* Cu
(Zn), Hcp	(Al,Cu,Zn)1	(Al,Cu,Zn)1	(ηZn) ≤419	hP2 *P6$_3$/mmc* Mg
θ, Al2Cu	(Al)2 (Al,Cu)1	(Al)2 (Al,Cu)1	θ, $CuAl_2$ ≤591	tI12 *I4/mcm* $CuAl_2$
η_1, Eta1	(Al,Cu)1 (Cu,Zn)1	"η" (Al,Cu)1 (Cu)1	η_1, CuAl(h) 624–560	oS32 [b] *Cmmm* $Cu_{0.94}Al_{0.94}$
η_2, Eta2	(Al)0.48 (Cu)0.52	"η" (Al,Cu)1 (Cu)1	η_2, CuAl(r) ≤561	mC20 *C2/m* CuAl(r)
ζ, Al9Cu11	(Al,Cu)9 (Cu)11	(Al)9(Cu)11	ζ_1, CuAl(h)[c] 590–530[a] Stable at 550 and 400 (10 days)[c]	oF88 Fmm2 $Cu_{47.8}Al_{35.5}$
ζ, Al9Cu11	(Al,Cu)9 (Cu)11	(Al)9(Cu)11	ζ_2, CuAl(r)[c] ≤570[a] Decomposes at 400 forming ζ_1[c]	oI24 Imm2 $Cu_{11.5}Al_9$
ε_1, Bcc	(Al,Cu,Zn)1	(Al,Cu,Zn)1	ε_1, CuAl 958–848	Cubic?
ε_2, Eps2	(Al,Cu,Zn)1 (Cu)1	(Al,Cu)1 (Cu)1	ε_2, CuAl 850–560	hP6 *P6$_3$/mmc* Ni_2In
δ_1, Al5Cu8	(Al)5(Cu)8	(Al)2(Cu)3	δ_1, CuAl	(hR*)
γ_2, Gamma2	(Cu)4 (Cu,Zn)6 (Al,Cu,Zn) 16	(Al,Cu,Zn)1	γ, Cu_5Zn_8 <835	cI52 *I-43m* Cu_5Zn_8
γ_2, Gamma2	(Cu)4 (Cu,Zn)6 (Al,Cu,Zn) 16	(Al,Zn)4 (Al,Cu,Zn)1 (Cu) 8	γ_0, CuAl 1037–800	cI52 *I-43m* Cu_5Zn_8
γ_1, Gamma1	(Cu)4 (Cu,Zn)6 (Al,Cu,Zn) 16	(Al,Cu,Zn)1	γ, Cu_9Al_4 <890	cP52 *P-43m* Cu_9Al_4
β, Bcc	(Al,Cu,Zn)1	(Al,Cu,Zn)1	β-CuAl 1049–559 β-CuZn (h) 903–454 β-CuZnAl	cI2 *Im-3m* W
β′, Bcc_B2	(Al,Cu,Zn)0.5 (Al,Cu,Zn) 0.5	(Al,Cu,Zn)0.5 (Al,Cu,Zn) 0.5	β′-CuZn (r) ≤468	cP2 *Pm-3m* CsCl
δ, Delta	(Al,Cu,Zn)1	(Al,Cu,Zn)1	δ, $CuZn_3$ 700–560	hP3 *P-6* $CuZn_3$
ε, Eps	(Al,Cu,Zn)1	(Al,Cu,Zn)1	ε, $CuZn_4$ ≤598	hP2 *P6$_3$/mmc* Mg
τ, Al5Cu4Zn	(Al,Cu)1 (Al)4(Cu)4 (Zn)1	(Al,Cu)1 (Al)4(Cu)4 (Zn) 1	τ, $Cu_5Zn_2Al_3$	≈cP2 CsCl

[a] Data and notation in the last two columns are generally from [7] which are accepted as assessment of experimental information.
[b] Crystal structure of η_1 is from [19].
[c] Crystal structure of ζ_1 and ζ_2 are from [20,21], discussed in detail in [6].

Table 2
Atomic distribution models for the γ_1 and γ_2 phases.

Model[a]	Cluster	IT 4 (8c)[b]	OT 4 (8c)	OH 6 (12e)	CO 12 (24 g)	References
A		**Zn**	**Cu**	**Cu**	**Zn**	[29,30]
B		(Cu, **Zn**)	(**Cu**, Zn)	**Cu**	**Zn**	[29]
C		**Zn**	**Cu**	(**Cu**,Zn)	(Cu, **Zn**)	[29,30]
D		(Al, Cu)	**Cu**	**Cu**	(Al, Cu)	[31]
E	E_0	(**Al,** Cu)	**Cu**	**Cu**	(Al, **Cu**)	[31]
	E_1	(Al, **Cu**)	**Cu**	**Cu**	(**Al,** Cu)	
F=C+D		(Al, Cu, Zn)	**Cu**	(**Cu**, Zn)	(Al, Cu, Zn)	[32,33]
G=C+E	G_0	(**Al,** Cu, Zn)	**Cu**	(**Cu**,Zn)	(Al, **Cu**, Zn)	This work
	G_1	(Al, **Cu,** Zn)	**Cu**	(**Cu**,Zn)	(**Al,** Cu, Zn)	

The majority species are given in bold font.
[a] A=(**Zn**)4(**Cu**)4(**Cu**)6(**Zn**)12, B=(Cu,**Zn**)4(**Cu**,Zn)4(**Cu**)6(**Zn**)12, and C=(**Zn**)4(**Cu**)4(**Cu**,Zn)6(Cu,**Zn**)12, A, B and C are for γ-CuZn (γ_2) phase, disordered only. D=(Al,Cu)4 (**Cu**)4(**Cu**)6(Al,Cu)12, for disordered γ-AlCu (γ_2) phase. E=(**Al**,Cu)2(Al,**Cu**)2(**Cu**)4(**Cu**)6(Al,**Cu**)6(**Al**,Cu)6, for ordered γ-AlCu (γ_1) phase. F=(Al,Cu,Zn)4(**Cu**)4(**Cu**,Zn)6(Al,Cu,Zn) 12, for ternary disordered γ (γ_2) phase. G=(**Al**,Cu,Zn)2(Al,**Cu**,Zn)2(**Cu**)4(**Cu**,Zn)6(**Al**,Cu,Zn)6(Al,**Cu**,Zn)6, for ternary ordered γ (γ_1) phase.
[b] The Wyckoff notation (8c, 8c, 12e, and 24g) for the 52 atoms unit cell is given in brackets.

structure), even though they possess different crystal structures. But in the text, Ghosh et al. [7] stated, in contrast, that "the solid solubilities of Al in Cu_5Zn_8 at 20 and 350 °C are about 3.5 and 7.0 mass% Al, respectively [15]. At the same temperatures, the γ_1 phases of the Al–Cu binary system dissolve about 30 mass% Zn [15]". Checked with all the original experimental work, we found

Table 3
Phase names; name in tdb-parameter file; models (sublattice formula), and parameters of the Gibbs energy equations for the ternary system developed in present work. Gibbs energy is given in J mol formula^{-1} and temperature (T) in Kelvin. Parameters for the binary sub-systems Al–Zn [27], Al–Cu [6], Cu–Zn [5], and the Gibbs energy equations using the same consistent notation [5,6] are not reproduced here.

Liquid; liquid; $(Al,Cu,Zn)_1$
$L^{0,Liq}_{Al,Cu,Zn} = 5475$
$L^{1,Liq}_{Al,Cu,Zn} = 13{,}000$
$L^{2,Liq}_{Al,Cu,Zn} = 43{,}800$

(Al), (Cu); Fcc; $(Al,Cu,Zn)_1$
$L^{0,Fcc}_{Al,Cu,Zn} = 90{,}000$
$L^{1,Fcc}_{Al,Cu,Zn} = 0$
$L^{2,Fcc}_{Al,Cu,Zn} = 90{,}000$

β, ε_1; Bcc; $(Al,Cu,Zn)_1$
$L^{0,Bcc}_{Al,Cu,Zn} = -10{,}000$
$L^{1,Bcc}_{Al,Cu,Zn} = -30{,}000+20\times T$
$L^{2,Bcc}_{Al,Cu,Zn} = -10{,}000$

(Zn); Hcp; $(Al,Cu,Zn)_1$
$L^{0,Hcp}_{Al,Cu} = 38{,}107$

γ_1; Gamma1; $(Cu)_4(Cu,Zn)_6(Al,Cu,Zn)_{16}$
$G^{0,Gamma1}_{Cu:Zn:Al} = 260{,}000+4\times G^{0,Fcc}_{Cu}+6\times G^{0,Hcp}_{Zn}+16\times G^{0,Fcc}_{Al}$
$G^{0,Gamma1}_{Cu:Cu:Zn} = -258{,}704-59.332\times T+10\times G^{0,Fcc}_{Cu}+16\times G^{0,Hcp}_{Zn}$
$G^{0,Gamma1}_{Cu:Zn:Cu} = 26{,}000+20\times G^{0,Fcc}_{Cu}+6\times G^{0,Hcp}_{Zn}$
$G^{0,Gamma1}_{Cu:Zn:Zn} = -36{,}316-112.4872\times T+4\times G^{0,Fcc}_{Cu}+22\times G^{0,Hcp}_{Zn}$
$L^{0,Gamma1}_{Cu:Cu:Al,Zn} = -574{,}960-200\times T$

γ_2; Gamma2; $(Cu)_4(Cu)_6(Al,Cu)_{16}$
$G^{0,Gamma2}_{Cu:Zn:Al} = -226{,}606+870\times T+4\times G^{0,Fcc}_{Cu}+6\times G^{0,Hcp}_{Zn}+16\times G^{0,Fcc}_{Al}$
$L^{0,Gamma2}_{Cu:Cu:Al,Zn} = -70{,}960-680\times T$

ε_2; Eps2; $(Al,Cu,Zn)_1(Cu)_1$
$G^{0,Eps2}_{Zn:Cu} = -8000+G^{0,Hcp}_{Zn}+G^{0,Fcc}_{Cu}$

η_1; Eta1; $(Al,Cu)_1(Cu,Zn)_1$
$G^{0,Eta1}_{Cu:Zn} = 3040+G^{0,Fcc}_{Cu}+G^{0,Hcp}_{Zn}$

ε; Eps; $(Al,Cu,Zn)_1$
$L^{0,Eps}_{Al,Cu} = -50{,}085$
$L^{0,Eps}_{Al,Zn} = 10{,}000$
$L^{0,Eps}_{Al,Cu,Zn} = 62{,}500$
$L^{1,Eps}_{Al,Cu,Zn} = -218{,}000$
$L^{2,Eps}_{Al,Cu,Zn} = 38{,}500$

τ; Al5Cu4Zn; $(Al,Cu)_1(Al)_4(Cu)_4(Zn)_1$
$G^{0,Al5Cu4Zn}_{Al:Al:Cu:Zn} = -368827.4+230\times T+5\times G^{0,Liquid}_{Al}+4\times G^{0,Liquid}_{Cu}+G^{0,Liquid}_{Zn}$
$G^{0,Al5Cu4Zn}_{Cu:Al:Cu:Zn} = -323713.2+118\times T+4\times G^{0,Liquid}_{Al}+5\times G^{0,Liquid}_{Cu}+G^{0,Liquid}_{Zn}$
$L^{0,Al5Cu4Zn}_{Al,Cu:Al:Cu:Zn} = 212280.2-300\times T$

that the first isothermal sections showing a continuous γ phase region were drawn by Bauer and Hansen [17]. They constructed several isothermal sections of Al–Cu–Zn ternary system in Cu-rich corner from 410 °C to 800 °C, but the compositions of their samples ended at the phase boundary of the β and γ phase. They proposed the continuous solid solution of the γ phase because they observed α+γ and β+γ two-phase regions and α+β+γ three-phase region along the γ phase region boundary. Actually, they did not work on a "single-phase" region of the γ phase. Later, Köster and Moeller [18] constructed the isothermal section at 350 °C. In principle they [18] accepted the statement of [17] with γ phase as a continuous solid phase. But their experimental results at 350 °C show that the structure of γ phase in Zn-poor side (i.e. near Al–Cu edge) is γ′-form, while in Zn-rich side (i.e. near Cu–Zn edge) is γ-form; the exact structure of γ and γ′ was not reported and "secondary structures γ_1 and γ_2 of the Al–Cu side" are included into that single-phase γ region. However, in their plotted 350 °C phase diagram section the continuous stripe of the γ phase connecting the binary edges is shown to be separated by a dashed line at 25 mass% Zn indicating a possibly higher order phase transition between the γ and γ′ structures [18].

In 1970s, Kandaurov et al. [15,16] reported two isothermal sections at 20 °C and 350 °C. Their results showed that the solid solubility of Al in γ-CuZn at 20 and 350 °C are about 3.5 and 7.0 mass% Al, respectively. At the same temperatures, the γ-AlCu phase dissolves about 30 mass% Zn [15]. They detected a wide two phase region between the γ-AlCu and γ-CuZn at room temperature and at 350 °C [15,16]. They also stated that the two γ phases may connect at higher temperature where γ-AlCu and γ-CuZn have the same crystal structure [15]. Kisi [22] reported that the alloy with composition of Cu64.8–Al28.3–Zn6.9 (at%) is single-phase at 400 °C, which agrees with the results of [16]. Kisi [22] also pointed out that to determine the crystal structure of the γ phase in Al–Cu–Zn ternary system would encounter several difficulties such as isolating single crystals and coping with the volatile zinc. More recently, some publications investigated the electron concentration and solid solution range of the γ phase, but focused on binary phases in Al–Cu and Cu–Zn [8,9].

According to the above discussion, we conclude that the information of complete solid solution of γ phase stems from the source of [17] and a simplification of [18], which are later widely cited in research works and reviews, such as [7]. On the other hand, the works of [15,16] were not acknowledged. Additionally, the experimental determination of the structural differences of the ternary γ phase is difficult [22]. Those may be the reasons why a simple single-phase solid solution range forming a complete stripe of the γ phase in the ternary system from 350 °C to 700 °C had been assumed in many works and in the review of [7]. In contrast, the experimental evidence is that the γ phase does not form a continuous ternary solid solution at 350 °C [15,16]. That is corroborated by the established fact that the binary edge compounds stable at 350 °C, γ_1 (Al–Cu, cP52 structure) and γ_2 (Cu–Zn, cI52 structure), possess different crystal structures. The constrained temperature–composition range at which γ_2 may form a continuous ternary solid solution starting from the Cu–Zn edge up to the high-temperature Al–Cu phase γ_2 with the same cI52 structure is still unknown.

In addition to that key distinction concerning γ phases the following differences and extensions of the ternary phase relations given in the review of [7] are pointed out.

The solid solubility ranges of Zn in Al–Cu binary compounds appear exaggerated in the assessed isothermal sections of [7], and no original experimental data could be found to support it.

Two ternary τ and τ′ phases are reported in [7] with possible formulas of $Cu_5Zn_2Al_3$ and Cu_3ZnAl_4, respectively. The τ phase is suggested to form in the maximum of a univariant eutectic reaction $L=\tau+\varepsilon_2$ at about 740 °C, while the τ′ phase appears at lower temperature and near the Al-rich end of the homogeneity range of the τ phase [7]. However, the original data on the τ and τ′ phases are partly contradictory and not conclusive [23–26]. More recent experimental work by Hao et al. [10] suggests that the τ′ phase

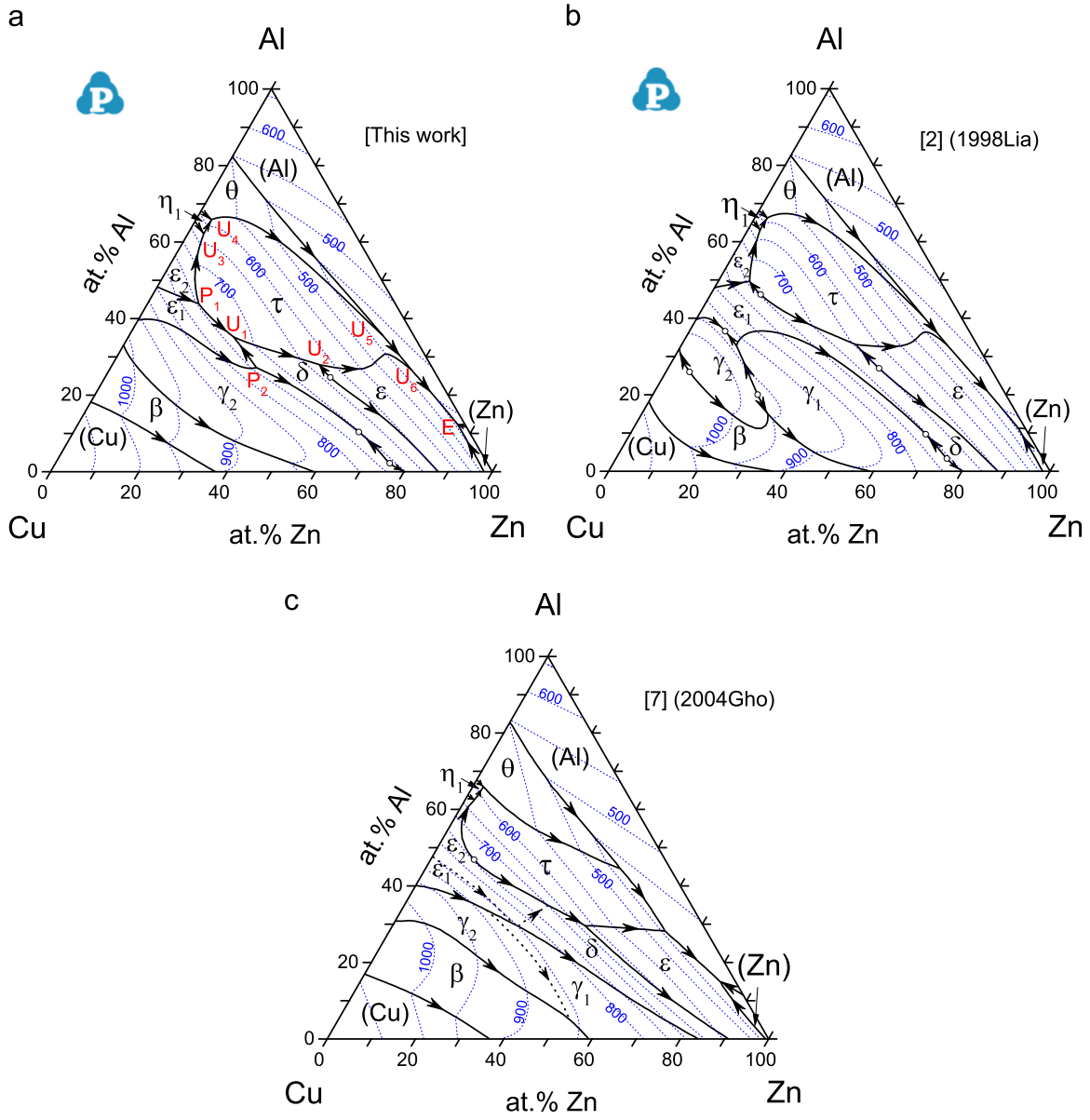

Fig. 1. Liquidus projection of the Al–Cu–Zn ternary system using the present phase notation: (a) calculated with the present dataset; (b) calculated with dataset from [2]; (c) manually assessed experimental liquidus projection redrawn from [7]. Isotherms are marked in °C. Additional shorthand-notation for references, indicating year and first author, is provided in brackets.

may be stable from room temperature to 400 °C with composition of Cu_4ZnAl_5, and even extend to the Al-richer corner [12].

Other recent work [11,13,14] studied the extension of the Fcc miscibility gap, (Al)′+(Al)″ from the Al–Zn binary system into the Al–Zn–Cu ternary system. The critical temperature of that miscibility gap of the Al–Zn system increases by the addition of Cu [14]. Borggren and Selleby [3] also report more recent experimental work on the phase equilibria in Cu-rich Al–Cu–Zn alloys for special brass application, not considered in [7].

3. Thermodynamic modeling

The thermodynamic descriptions of the binary edge systems are taken from Al–Zn [27], Al–Cu [6], and Cu–Zn [5]. For details of the unary data, the Gibbs energy equations and the thermodynamic models of the solution phases and the binary compounds the reader may refer to Part I [5] and Part II [6] of this series.

For the Al–Zn binary the more recent assessment by Kogo and Hirosawa [28], published in 2014, as compared to the work of Mey from 1993 [27], was not accepted. The main contribution of [28] is the introduction of elastic coherency strain energy to calculate the so-called “coherent miscibility gap”, which is not considered in this work. However, the basic thermodynamic parameters of the Al–Zn system have also been changed by [28], starting from the values of [27]. This change constitutes a significant deterioration as obvious from Fig. 1 of [28] (deviation of solidus line from experimental data, eutectoid temperature too high) and Fig. 4 of [28] the chemical potential of Al in Fcc at 380 °C. Therefore, we have used the superior assessment of the Al–Zn system by Mey [27].

Table 4
Temperatures and compositions of the liquid at the invariant equilibria calculated in this work (bold font) compared with assessed experimental data [7] and previous Calphad calculation by Liang and Chang [2].

Reaction	Type	Temperature (°C)	Liquid composition			Reference
			at% Al	at% Cu	at% Zn	
$L+\varepsilon_2+\varepsilon_1 \leftrightarrow \tau$	**P_1**	**742**	**43.9**	**44.5**	**11.6**	**[This work] Calc.**
$L+\varepsilon_1 \leftrightarrow \tau+\varepsilon_2$		737	49.6	43.5	6.9	[2] Calc.
$L+\varepsilon_1+\gamma_2 \leftrightarrow \delta$	**P_2**	**734**	**27.2**	**39.8**	**33.0**	**[This work] Calc.**
$L+\varepsilon_1 \leftrightarrow \tau+\delta$	**U_1**	**718**	**35.2**	**40.9**	**23.9**	**[This work] Calc.**
$L+\delta \leftrightarrow \varepsilon+\tau$	**U_2**	**625**	**27.9**	**25.1**	**47.0**	**[This work] Calc.**
$L+\delta+\tau \leftrightarrow \varepsilon$		625	29.7	26.9	43.4	[7] Exp.
$L+\delta \leftrightarrow \varepsilon+\tau$		644	33.1	27.4	39.5	[2] Calc.
$L+\varepsilon_2 \leftrightarrow \eta_1+\tau$	**U_3**	**620**	**62.2**	**34.2**	**3.6**	**[This work] Calc.**
		620	62.6	35.2	2.2	[7] Exp.
		620	62.8	34.3	2.0	[2] Calc.
$L+\eta_1 \leftrightarrow \theta+\tau$	**U_4**	**578**	**65.9**	**30.6**	**3.5**	**[This work] Calc.**
		580	65.9	31.6	2.5	[7] Exp.
		580	66.8	31.2	2.0	[2] Calc.
$L+\theta \leftrightarrow (Al)+\tau$	**U_5**	**422**	**35.7**	**7.0**	**57.2**	**[This work] Calc.**
		422	44.5	11.3	44.2	[7] Exp.
		425	40.9	8.6	50.5	[2] Calc.
$L+\tau \leftrightarrow (Al)+\varepsilon$	**U_6**	**411**	**26.7**	**5.0**	**68.3**	**[This work] Calc.**
		396	28.2	9.4	62.4	[7] Exp.
		421	33.1	6.8	60.1	[2] Calc.
$L \leftrightarrow (Al)+(Zn)+\varepsilon$	**E**	**379**	**12.2**	**1.6**	**86.1**	**[This work] Calc.**
		377	15.4	3.7	80.9	[7] Exp.
		381	11.2	1.6	87.2	[2] Calc.

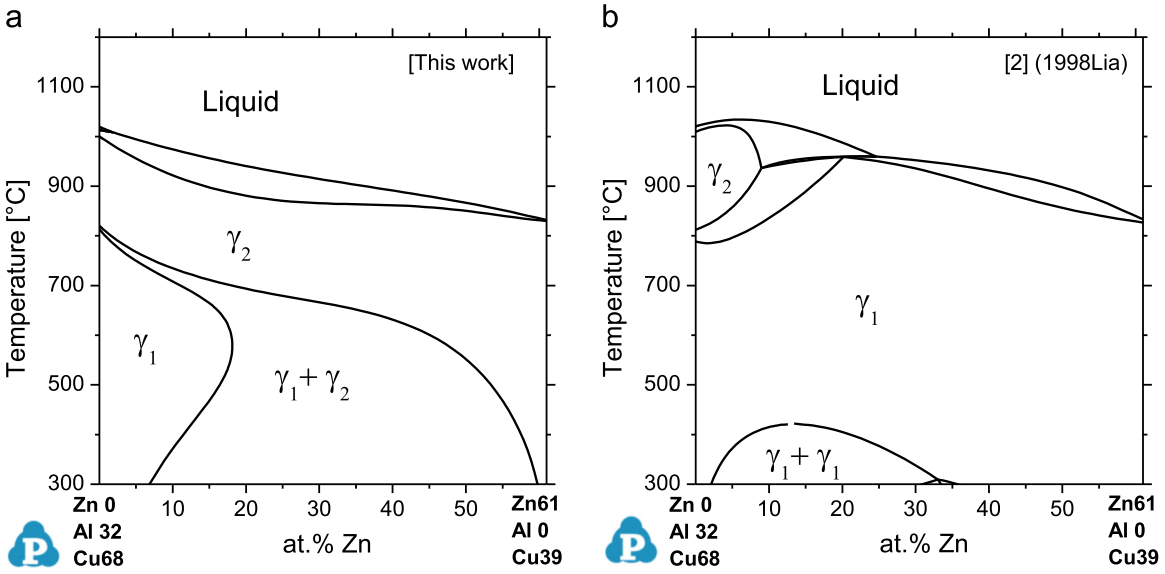

Fig. 2. The calculated vertical phase diagram section of Al–Cu–Zn system along the composition line from Al32Cu68 to Cu39Zn61 (at%) reveals the phase regions of the γ phases: (a) this work; (b) calculated with dataset from [2].

Further explanation of selecting the model of the γ phases is required because of their complexity. For the binary edge systems the descriptions of the ordered phase γ_1 (Al–Cu, low-T, cP52) and the disordered phase γ_2 (Al–Cu, high-T, cI52) and γ_2 or γ (Cu–Zn, cI52) are given in [5,6]. Table 2 shows the atomic distribution of the elements in the binary Cu–Zn (models A, B, and C) [29,30],

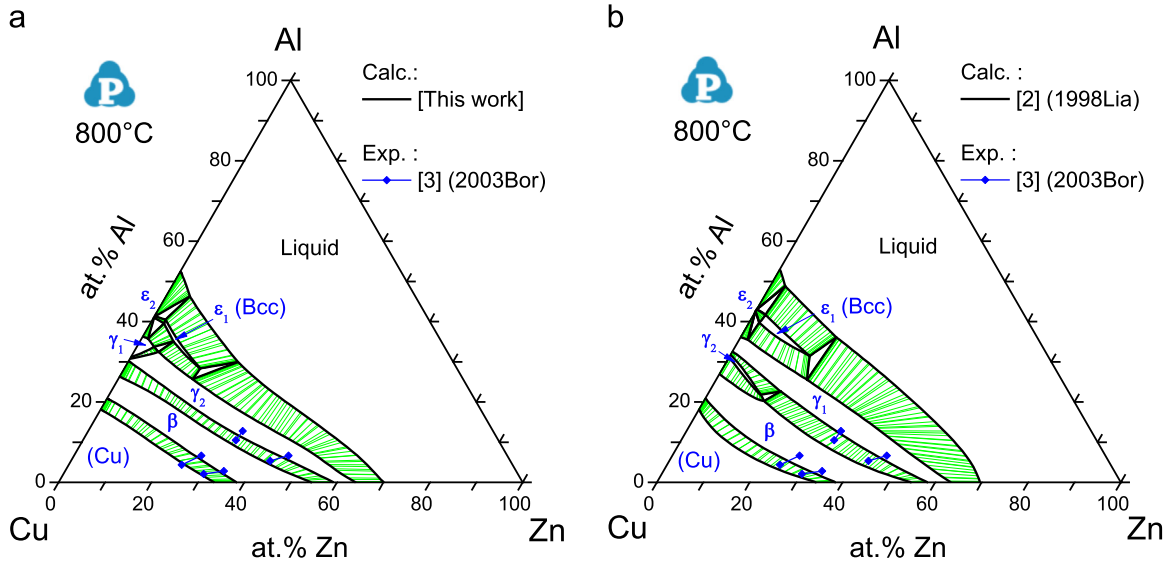

Fig. 3. Comparison of the calculated isothermal Al–Cu–Zn section at 800 °C with the experimental data from [3]: (a) this work; (b) calculation with dataset from [2].

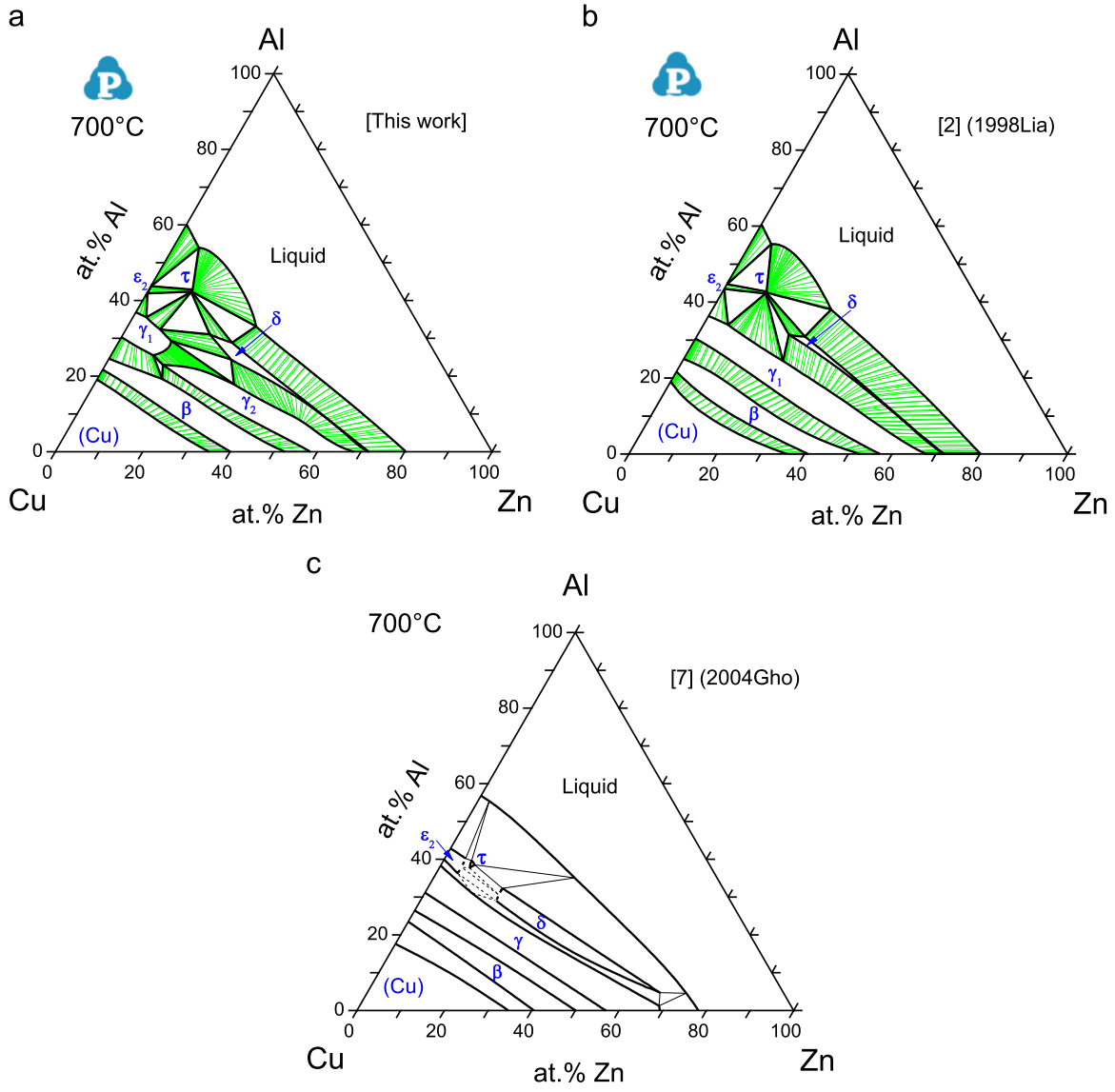

Fig. 4. Isothermal Al–Cu–Zn section at 700 °C. (a) Calculated with the present dataset; (b) calculated with dataset from [2]; (c) experimental assessment from [7].

binary Al–Cu (models D and E) [31] and ternary γ phases (models F and G) considered in this work.

The binary ordered γ-AlCu phase (γ_1), with prototype of Cu_9Al_4, is cP52 structure in the space group of *P-43m* [31]. The crystal structure of the ordered γ-AlCu phase is composed of two clusters of 26 atoms to form the CsCl-type structure. The 26 atoms in the cluster are distributed over four vertices of an inner tetrahedron (IT), four vertices of an outer tetrahedron (OT), six vertices of an octahedron (OH) and 12 vertices of a cubo-ochtahedron (CO). The atom distribution in the two clusters (E_0 and E_1) is shown as model E in the Table 2. In the cluster E_0, Al is the major element in inner tetrahedron (IT) positions while Cu is majority in cubo-octahedron (CO) positions; it is the just the opposite situation with Al majority in CO position and Cu majority in IT positions in the cluster E_1 [31]. This corresponds to the six-sublattice model E=(**Al,** Cu)2(Al,**Cu**)2(**Cu**)4(**Cu**)6(Al,**Cu**)6(**Al,**Cu)6 for the ordered γ-AlCu (γ_1) phase. Here the majority species are highlighted by bold font indicating that the site fractions on the first and second sublattice, (**Al,**Cu)2(Al,**Cu**)2, comprising the four (IT) positions, are different. Upon disordering the first and second sublattice (IT) as well as the fifth and sixth sublattice (CO) merge to define the four-sublattice model D=(Al,Cu)4(**Cu**)4(**Cu**)6(Al,Cu)12 for the disordered γ-AlCu (γ_2) phase.

The binary γ-CuZn (γ_2) phase is stable in the disordered form only. It is agreed upon [29,30] that among the possible models A, B, and C the latter is most suitable. This corresponds to the four-sublattice model C=(**Zn**)4(**Cu**)4(**Cu**,Zn)6(Cu,**Zn**)12.

In the ternary system, according to the best known crystal structure, the disordered phase γ (or γ_2) should be modeled as (Al, Cu,Zn)4(**Cu**)4(**Cu**,Zn)6(Al,Cu,Zn)12, model F, resulting from combining models C and D. That model option was also recommended in [32] and discussed in the 1997 Ringberg workshop [33]. However, it was never applied in any published thermodynamic description because of its complexity; it involves $3 \times 2 \times 3 = 18$ end

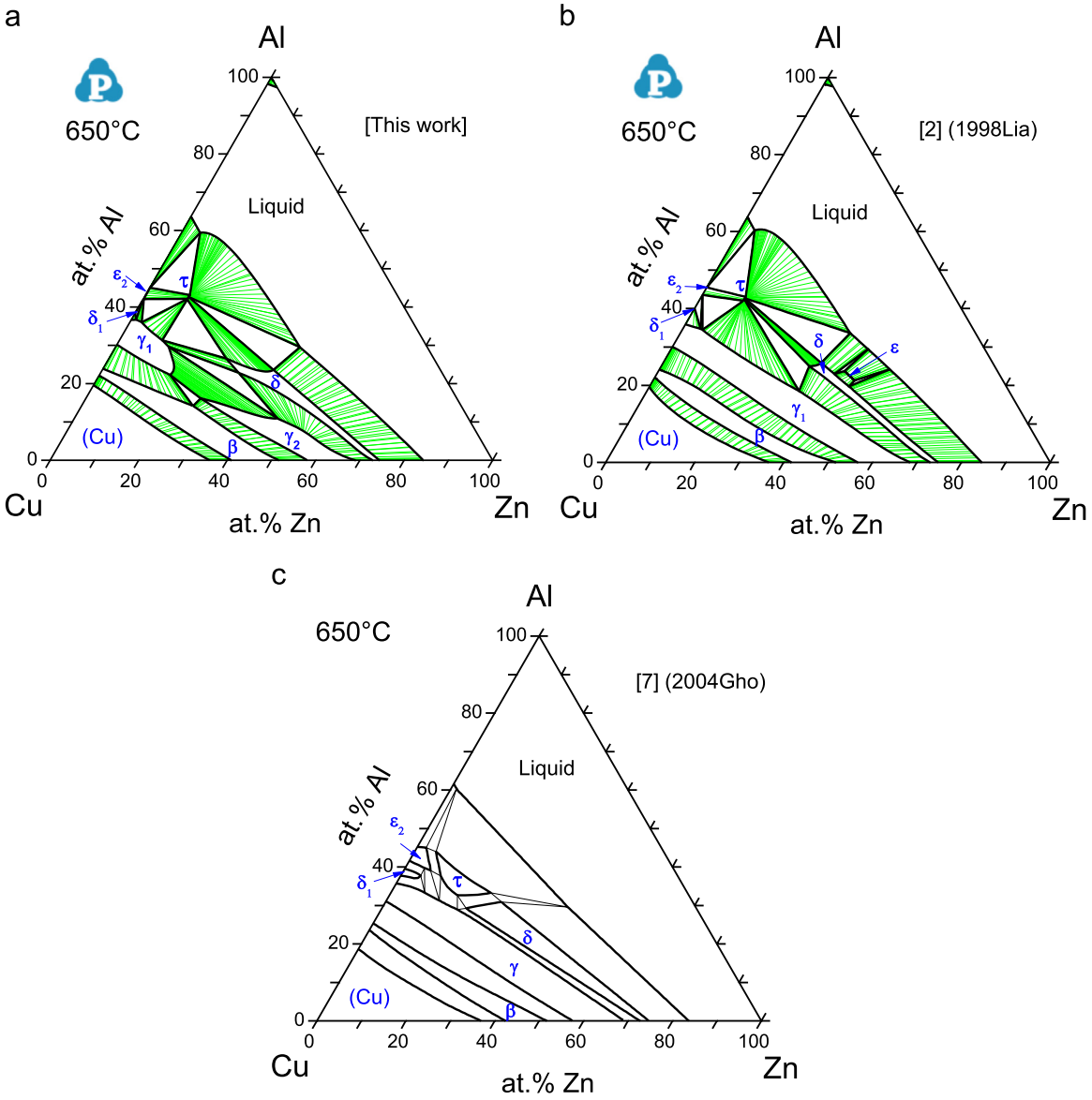

Fig. 5. Isothermal Al–Cu–Zn section at 650 °C. (a) Calculated with the present dataset; (b) calculated with dataset from [2]; (c) experimental assessment from [7].

member parameters, not counting possible interaction parameters. We suggest to combine the two (Al,Cu,Zn) sublattices (IT and CO) and simplify it to the three-sublattice model (**Cu**)4(**Cu**,Zn)6(Al,Cu,Zn)16, which only involves 6 end members for the present model of the disordered phase γ_2.

The ordered phase γ (or γ_1) in the ternary system may be formed by starting with model E and introducing Zn from model C to occupy some sites in IT, OH, and CO positions, as shown by model G. That corresponds to the very complex six-sublattice model of G=(**Al,**Cu,Zn)2(Al,**Cu**,Zn)2(**Cu**)4(**Cu**,Zn)6(Al,**Cu**,Zn)6(**Al**,Cu,Zn)6 with 162 end members. That explains why, in the present work, we will not model the γ_1/γ_2 transition as order–disorder transition but rather use separate phase descriptions. Therefore, we again combine the sublattices IT and CO, all containing (Al,Cu, and Zn) atoms, to the three-sublattice model (**Cu**)4(**Cu**,Zn)6(Al,Cu,Zn)16 for the present model of the ordered phase γ_1. It is seen that, formally, this is the same model as for the disordered γ_2 phase.

In conclusion, in this work we model the γ_2 phase in the ternary by joining the disordered γ_2-AlCu phase, which is the high-temperature Al–Cu phase (named as γ_0 in [7,34]), and the γ(γ_2)-CuZn phase, which is of the same disordered structure. As a separate γ_1 phase in the ternary we model the ordered low-temperature γ_1-AlCu phase with significant, though limited, solubility of Zn. Both γ_1 and γ_2 phases are described by the simplified three-sublattice model (**Cu**)4(**Cu**,Zn)6(Al,Cu,Zn)16. That approach involves only 12 (twice 6) end members as opposed to 162 end members necessary for the crystallographically more exact model of the ternary γ_1/γ_2 phases (G) by an order–disorder transition.

Liang and Chang [2] connected the γ-CuZn phase with the low-temperature γ-AlCu phase, not acknowledging the different crystal structures, and modeled this phase with a simple single sublattice model, (Al,Cu,Zn). For the high-temperature "γ_0"-CuAl phase they accepted the binary model of [35], (Al)4(Al,Cu)1(Cu)8, and modified it by introducing Zn in the model (Al,Zn)4(Al,Cu,Zn)1(Cu)8.

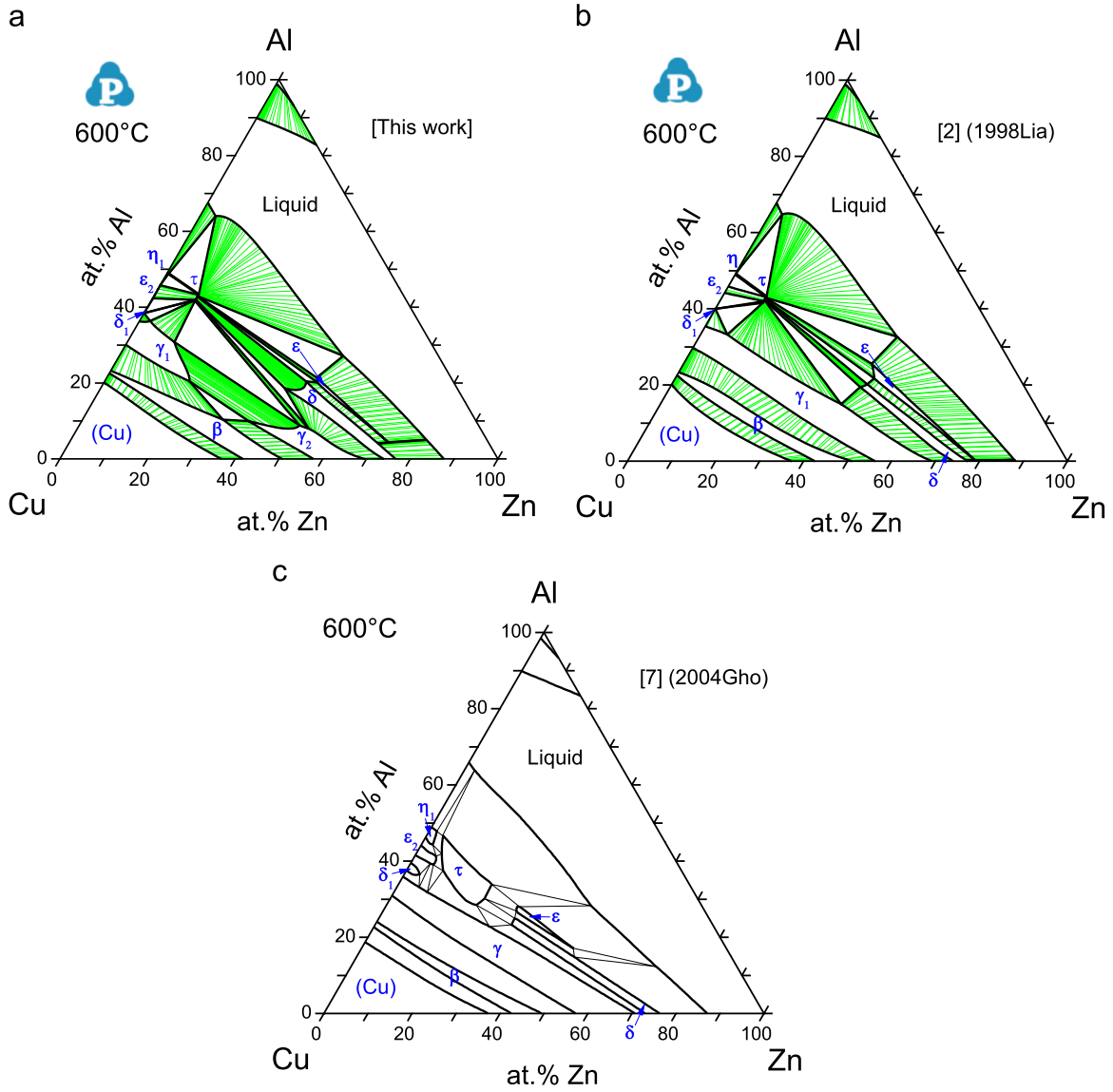

Fig. 6. Isothermal Al–Cu–Zn section at 600 °C. (a) Calculated with the present dataset; (b) calculated with dataset from [2]; (c) experimental assessment from [7].

However, the binary model (Al)4(Al,Cu)1(Cu)8 for "γ_0" [35] has no relation to the crystal structure whatsoever and is just a simple way to constrain the composition range, as discussed in Part II [6]. In order to get a reasonable description of the ternary experimental phase equilibria, Liang and Chang [2] used 19 parameters for the two γ phases: 10 binary and ternary interaction parameters together with 3 end member parameters for the "γ" phase and 6 end member parameters for a separate high temperature "γ_0"-AlCu (named γ_2 in this work). In the present work we used 18 parameters in total, 6 end members and 3 interaction parameters, for both γ phases.

The Al–Cu–Zn ternary τ and τ′ phase is treated here as one phase with a three sublattice model accepted from [2]. The experimental results on this ternary phase are not conclusive and we cannot make a better judgment than [2].

Thermodynamic calculations and the parameter optimization are performed using the Pandat software package (www.computherm.com) with PanOptimizer [36]. All thermodynamic Gibbs energy parameters determined in the present work are given in Table 3. The complete ternary thermodynamic database is also given as Supplementary TDB file.

4. Results and discussion

4.1. Liquidus projection and invariant reactions

Fig. 1 shows the liquidus projection of Al–Cu–Zn ternary system. Compared to the previous calculation, Fig. 1b [2], the monovariant line of the L+(Cu)+β equilibrium in the Cu-rich corner calculated in this work (Fig. 1a) agrees better with the experimental data (Fig. 1c).

Indicating a lack of experimental information, the assessed experimental liquidus projection (Fig. 1c) shows three dashed monovariant lines at the central part of the diagram: the monovariant lines of L+γ_1+γ_2, L+ε_1+ε_2, and L+$\varepsilon_{1/2}$+δ. In this work the ε_1 and δ phase are modeled as two separate phases, because the ε_1 phase is of cubic structure whereas the δ phase is of

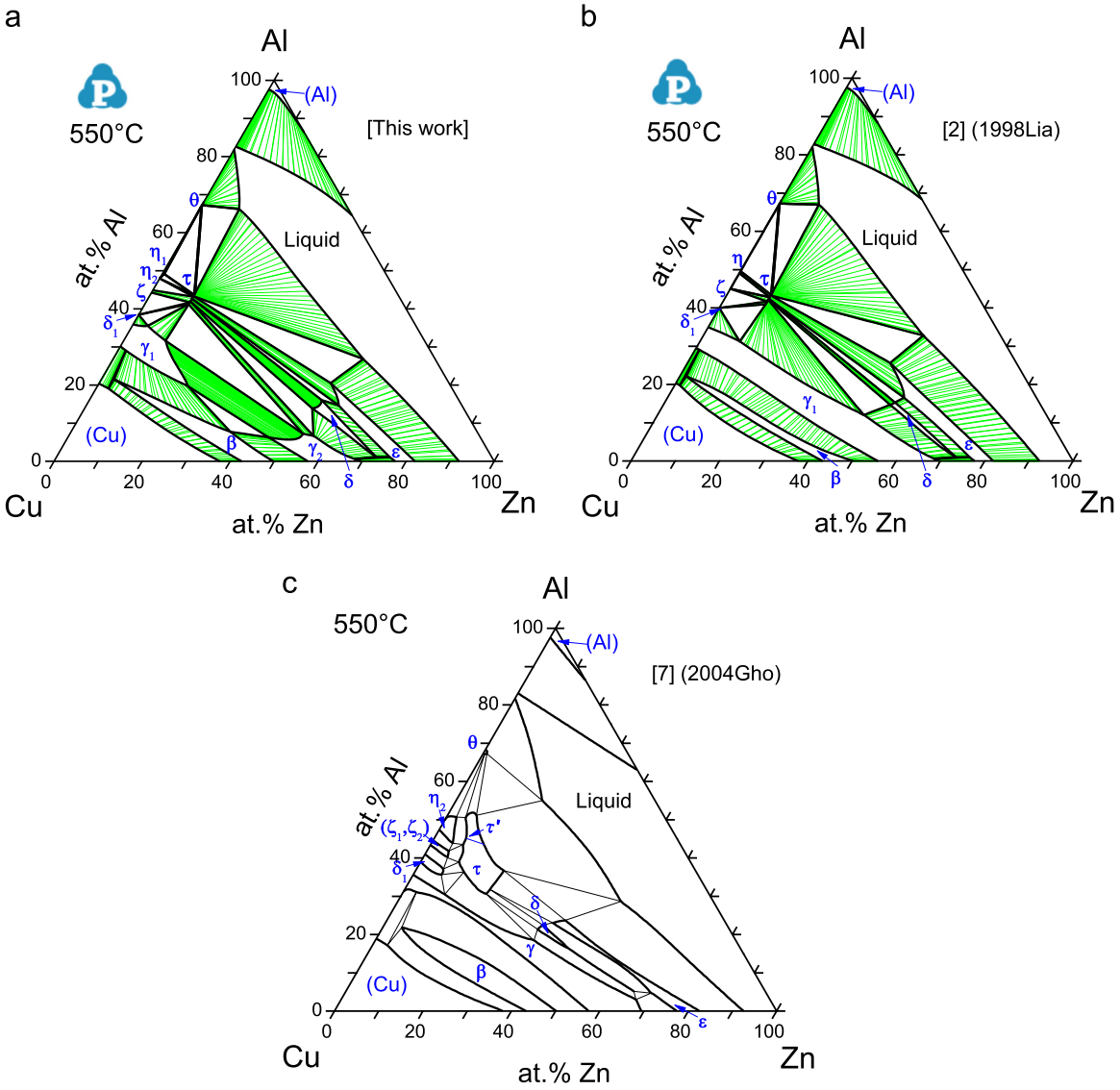

Fig. 7. Isothermal Al–Cu–Zn section at 550 °C. (a) Calculated with the present dataset; (b) calculated with dataset from [2]; (c) experimental assessment from [7].

hexagonal structure. That was discussed in detail in Part I [5], thus a monovariant line appears between ε_1 and δ primary phase regions in Fig. 1a. The thermodynamic descriptions of Al–Cu binary system in [35] and Cu–Zn binary system in [37] were adopted in [2], where both ε_1 and δ phases are Bcc phase, so no monovariant line between them appears in the liquidus projection in Fig. 1b. It is noted that for convenience the phase notations ε_1 and β are maintained in Fig. 1a, even though both are modeled as the same phase Bcc.

The 9 invariant reactions involving the liquid phase calculated in this work are compared with those calculated with the dataset of [2] and the experimental results [7] in Table 4. In the second column only the reaction type obtained in this work is indicated to emphasize that literature data shown in following lines, if available, belong to the same four-phase equilibrium. For the reactions calculated at the three highest temperatures, 742, 734, and 718 °C in this work there are no experimental data to compare with.

Different reaction types are obtained for reaction U_2 calculated at 625 °C as $L+\delta \leftrightarrow \varepsilon+\tau$ it is a transition type reaction (U) in this work, while it was assessed as $L+\delta+\tau \leftrightarrow \varepsilon$, a ternary peritectic reaction (P) in [7]. However, the calculated invariant reaction temperature in this work is the same as the experimental value of 625 °C, compared to 644 °C calculated by [2]. The liquid phase composition calculated in this work is also in better agreement with the experimental data.

Compared to the composition, we put more weight on the temperature of invariant reactions, because the invariant reaction temperature can be determined experimentally more accurately than the composition of the liquid phase. For invariant temperatures our calculation is always closer to the experimental data compared to Ref. [2], except U_3 and U_4 which are in same agreement. Specifically, for equilibria U_5 and E, our calculations are in good agreement with the experiment results. For equilibrium U_6, even though our calculation is 15 K above the experimental data, it is still in better agreement compared to the previous thermodynamic description [2], which is 25 K higher.

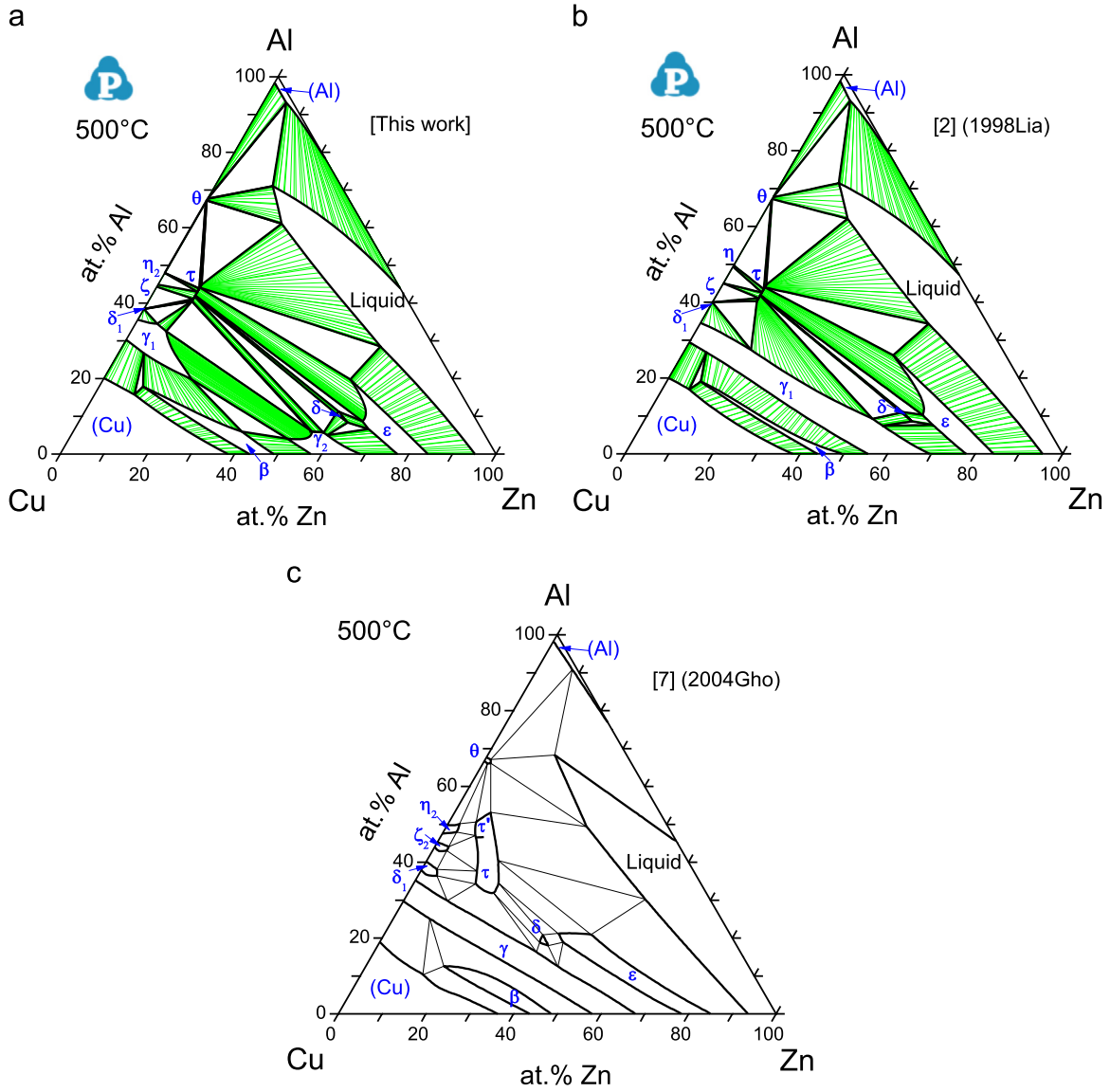

Fig. 8. Isothermal Al–Cu–Zn section at 500 °C. (a) Calculated with the present dataset; (b) calculated with dataset from [2]; (c) experimental assessment from [7].

4.2. The γ phases

In this work, the high temperature γ-AlCu phase (cI52 structure) is modeled as the same phase as the γ-Cu_5Zn_8 phase (cI52 structure) because of their same crystal structure, and named as γ_2 phase. So only the γ_2 phase shows a primary crystallization field in the calculated liquidus projection, Fig. 1a, and no monovariant line exists in that field from the Cu–Zn side to the Al–Cu side. In [2], on the contrary, the γ-Cu_5Zn_8 phase (cI52 structure) connects with the low temperature γ-Cu_9Al_4 (cP52 structure) phase, named as γ_1 phase, while the high temperature γ-AlCu phase (cI52 structure) was modeled as a separate γ_2 phase. Therefore, a monovariant line appears between the γ_1 and γ_2 primary phase regions in Fig. 1b.

In order to better understand this key distinction and the phase regions of the two γ phases, Fig. 2 represents the vertical section of the Al–Cu–Zn phase diagram along the composition cut from Al32Cu68 to Cu39Zn61 (at%), which cuts through the γ phases from the Al–Cu to the Cu–Zn edge. In this work, Fig. 2a, the high temperature γ_2-AlCu phase (disordered phase) connects with the γ-CuZn phase, thus consistently named as γ_2 phase, because both are the disordered phase with the same structure, cI52. The low temperature γ_1-AlCu phase (ordered phase with cP52 structure) shows limited extension into the ternary. Between the γ_1 and γ_2 phase a two-phase region exists, because we did not consider the order–disorder transition, known in the Al–Cu binary, see Part I [5], but treated them as two separate phases.

In the work of Liang and Chang, on the contrary, the low temperature γ_1-AlCu phase (cP52 structure) is modeled as joint phase with γ-CuZn phase (cI52 structure) named as the γ or γ_1 phase in [2]. As shown in Fig. 2b, their γ_1 phase shows the complete solid solution range between 420 °C and 785 °C, but has a spinodal miscibility gap at temperature below 420 °C. The solubility of Zn in their γ_2 phase (cI52) is limited to about 8 at% Zn and the liquidus shows a peculiar maximum in that range, see Fig. 2b.

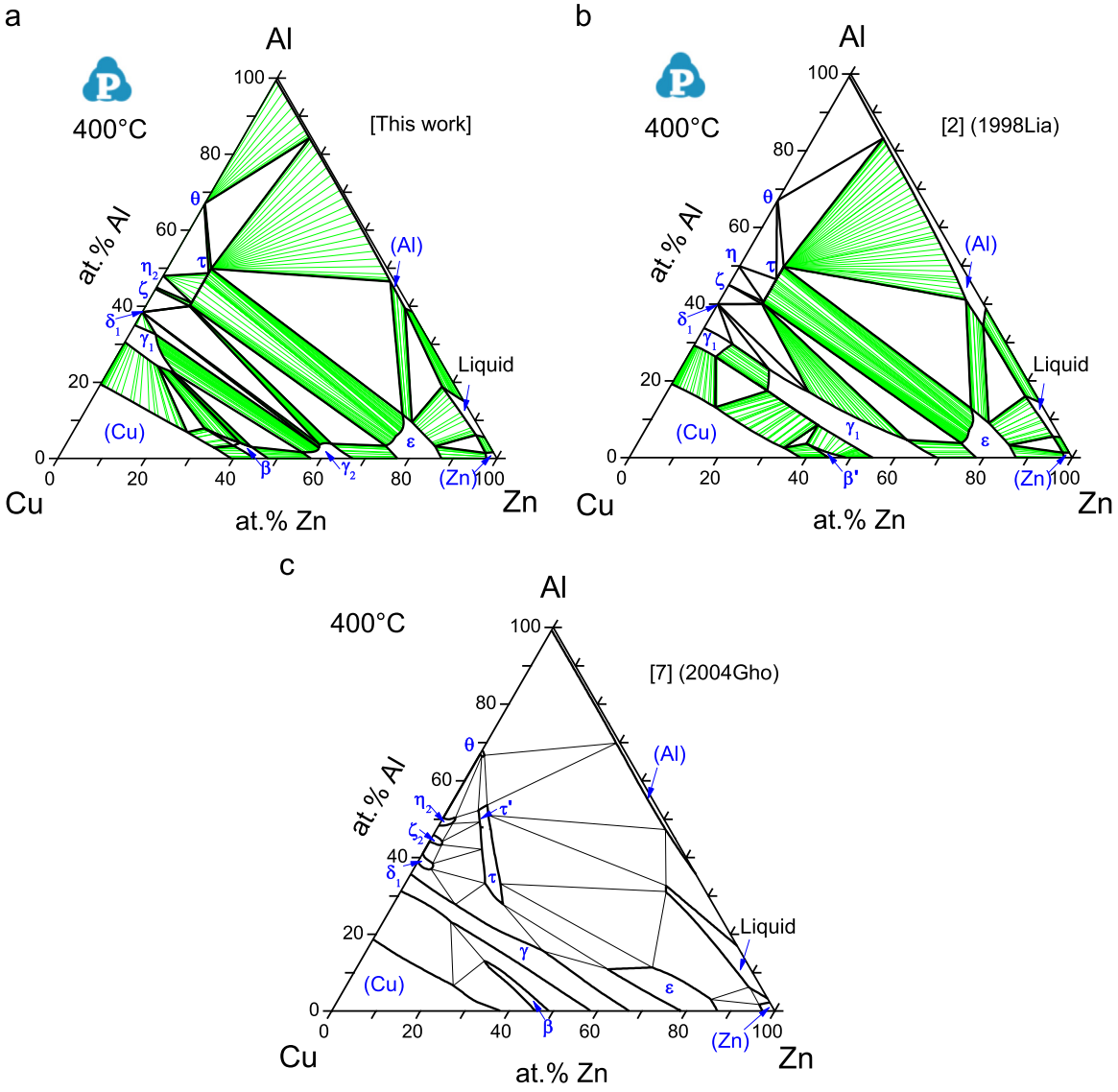

Fig. 9. Isothermal Al–Cu–Zn section at 400 °C. (a) Calculated with the present dataset; (b) calculated with dataset from [2]; (c) experimental assessment from [7].

4.3. Isothermal sections

Fig. 3 represents the isothermal section at 800 °C calculated from the present work (a) and previous thermodynamic description [2] (b), both in comparison with recent experimental data [3]. The present work (Fig. 3a) shows better agreement with the experimentally determined [3] tie-lines (Cu)+β and β+γ_2 compared to the calculation of [2] shown in Fig. 3b. In this 800 °C section it is also clearly seen that the γ_2 phase is continuous from the Cu–Zn to the Al–Cu side. This continuous γ_2 phase is in equilibrium with the continuous β phase through the continuous β+γ_2 two-phase region in this work (Fig. 3a). The γ_1+γ_2 two-phase region is very narrow and, thus, approximately resembles the γ_1/γ_2 order–disorder transition known in the Al–Cu binary.

In the isothermal section calculated from [2] (Fig. 3b), the γ_1 phase was chosen as the continuous solid solution phase from the Al–Cu to the Cu–Zn binary system, in conflict with the different crystal structures. The separate γ_2 phase penetrates deep into the ternary system up to 11.8 at% Zn, forming a wide γ_1+γ_2 two-phase region ending at the γ_1+γ_2+β tie-triangle. The direction and width of the γ_1+γ_2 two-phase region in [2] appears unlikely and is probably not a good approximate for the γ_1/γ_2 order–disorder transition, although no experimental data are available for comparison.

Figs. 4–11 provide the comprehensive comparison of the isothermal sections calculated from the present work (a), the previous calculations [2] (b), and assessed experimental phase diagrams [7] (c). The main differences between the calculations of this work and the previous description [2] are seen around the γ phase regions. With decreasing temperature, the calculated isothermal sections in this work show γ_1+γ_2 two phase region between the γ_1 phase (cP52 structure) from Al–Cu side and the γ_2 phase (cI52 structure) from Cu–Zn side. The assessed experimental phase diagrams in [7] assumed that "γ" phase forms a complete solid solution range from Al–Cu to Cu–Zn between 700 °C and 350 °C, which is disapproved in this work as detailed above in Section 2.

In fact, a γ_1+γ_2 two phase region was experimentally determined in the isothermal sections at room temperature and 350 °C [15,16]. This key information was only mentioned in the

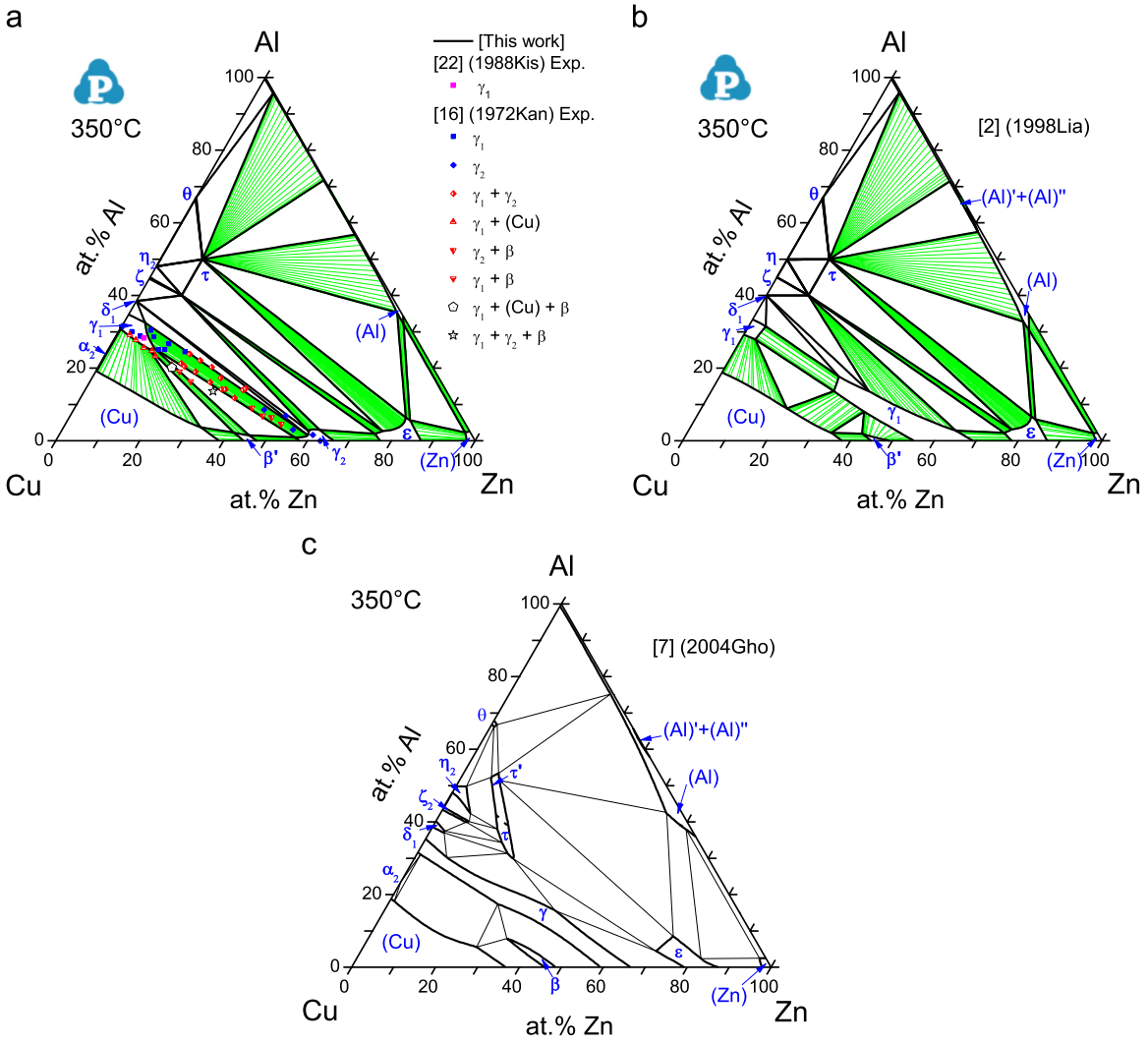

Fig. 10. Isothermal Al–Cu–Zn section at 350 °C. (a) Calculated with the present dataset and compared with experimental data from [16,22]. (b) Calculated with dataset from [2]; (c) experimental assessment from [7].

text rather than reflected in the plotted phase diagrams of the review of [7]. Fig. 10a represents the calculated isothermal section compared with the original experimental results from [16] at 350 °C. The two key samples located in the $\gamma_1+\gamma_2+\beta$ and $\gamma_1+(Cu)+\beta'$ three-phase regions detected in [16] agree well with the present calculation. The presently calculated solid solubility of the third element in both γ phases, i.e. Zn in γ_1 and Al in γ_2, are less than the experimental values, however, the existence of the key two-phase equilibrium $\gamma_1^{Al\text{-}rich}+\beta'$ agrees with our calculation. In contrast, in the calculation with the dataset of [2], Fig. 10b, the missing $\gamma_1^{Al\text{-}rich}+\beta'$ tie-lines and the calculated $(Cu)+\gamma_1^{Al\text{-}rich}+\gamma_1^{Zn\text{-}rich}$ and $(Cu)+\gamma_1^{Zn\text{-}rich}+\beta'$ three-phase regions disagree with the key experimental results [15,16].

In the isothermal section at 300 °C, a small miscibility gap in the (Cu) phase, Fcc′+Fcc″, appears calculated with datasets from [2] (Fig. 11b). The calculated result in this work (Fig. 11a) agrees with the experimental phase diagram (Fig. 11c) which shows no miscibility gap. However, one should realize that in the metastable Al–Cu–Zn ternary system, constrained to the Fcc phase, a "rose" phase diagram with Fcc-demixing exists, as discussed in [38]. This is probably due to the well-known stable Fcc′+Fcc″ gap emerging from the Al–Zn binary and a metastable Fcc′+Fcc″ gap emerging from the Al–Cu binary. In the present work, a small stable part of this miscibility gap will also appear at the (Cu) phase region at temperature below 220 °C. The calculated results in the present work also support the experimental result that small additions of Cu to Al–Zn alloys increase the critical temperature of the stable Fcc′+Fcc″ miscibility gap, also denoted as (Al)′+(Al)″ [14].

4.4. Vertical sections

Fig. 12 presents the vertical phase diagram sections at constant 2, 4, and 6 mass% Al in good agreement with the experimental liquidus and solidus temperatures [17]. Significant improvement compared to the work of Liang and Chang [2] is achieved. Actually,

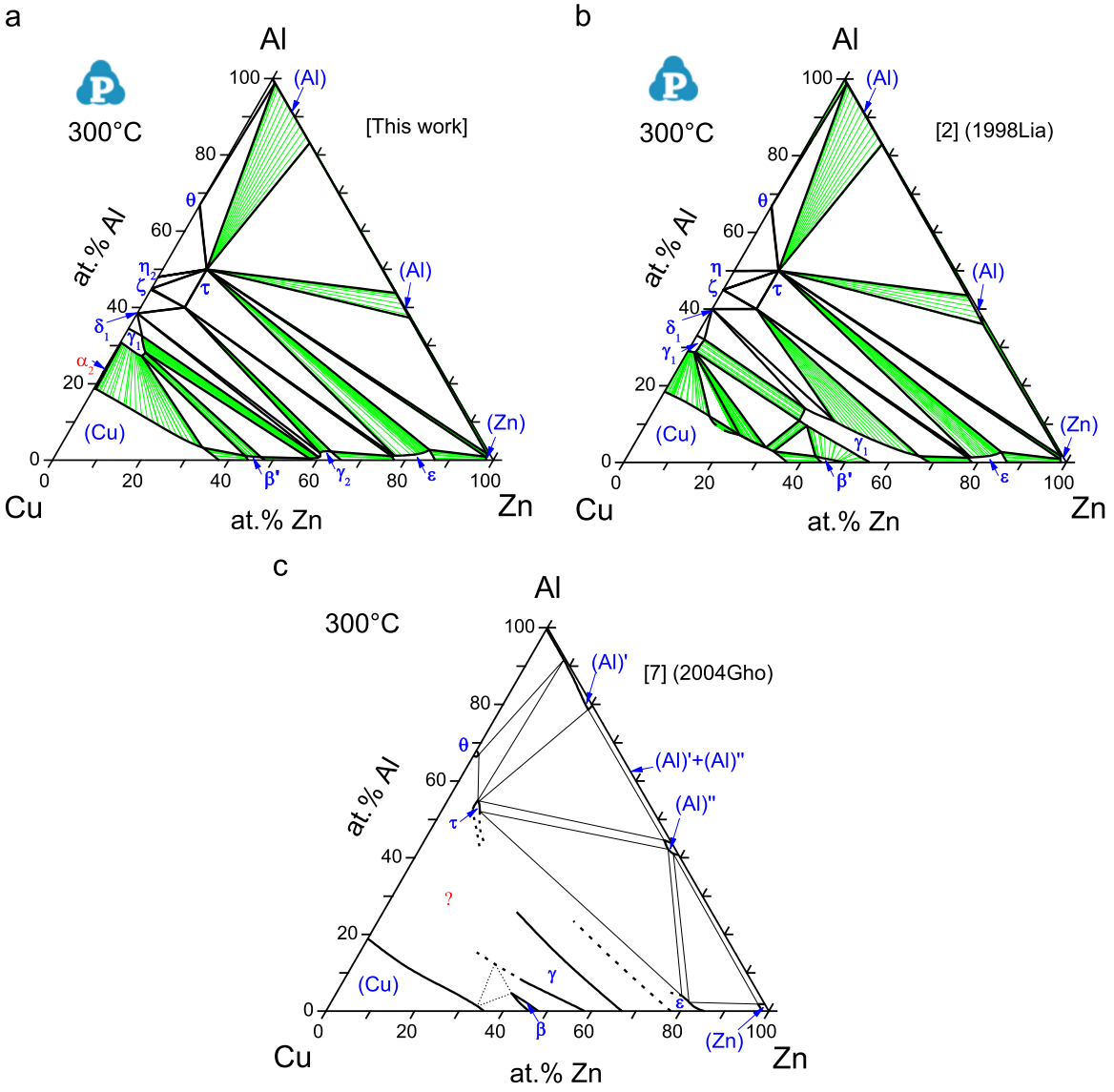

Fig. 11. Isothermal Al–Cu–Zn section at 300 °C. (a) Calculated with the present dataset; (b) calculated with dataset from [2]; (c) experimental assessment from [7].

this improved description of the liquidus temperatures is consistent with the better description of the liquidus projection in this work as shown in Fig. 1. The presently calculated solid phase regions in these phase diagrams fit with all the experimental data [17] in Fig. 12a, but not in Fig. 12b and c; however, a general improvement compared to [2] is also noted in the solid state equilibria of Fig. 12a–c.

Köster [39] presented some original experimental phase boundary data in six vertical phase diagram sections of the Al–Cu–Zn phase diagram. A selection of these data in the sections at constant 20 mass% Cu, 20 mass% Zn, and 40 mass% Zn has been shown in comparison to the calculated diagrams in [2], which are also shown in Fig. 13. The present calculation is generally close to the previous calculation [2] of these sections. Compared to the previous calculation [2], the presently calculated temperatures of invariant reactions associated with (Al)+τ+ε (U_6) and (Al)+τ+θ (U_5) are closer to the experimental data, which can be seen from Fig. 13a and b, respectively. Moreover, it is noted that all of these experimental data from [17,39] have been considered and converted in the assessment procedure by which the set of experimental isothermal sections was generated in [7], which were mainly used for comparison to calculated diagrams in this work.

4.5. Thermodynamic properties of liquid phase

Fig. 14 compares the chemical potentials of Al at 700, 750, and 800 °C in the liquid state for the section at constant 7.5 at% Cu calculated from the present work with the experimental values of [40] and previous calculation [2]. Fig. 15 shows comparisons of the calculated activities of Zn in the liquid state with the experimental values of [41] and calculated values of [2] at 1100 °C (a) and

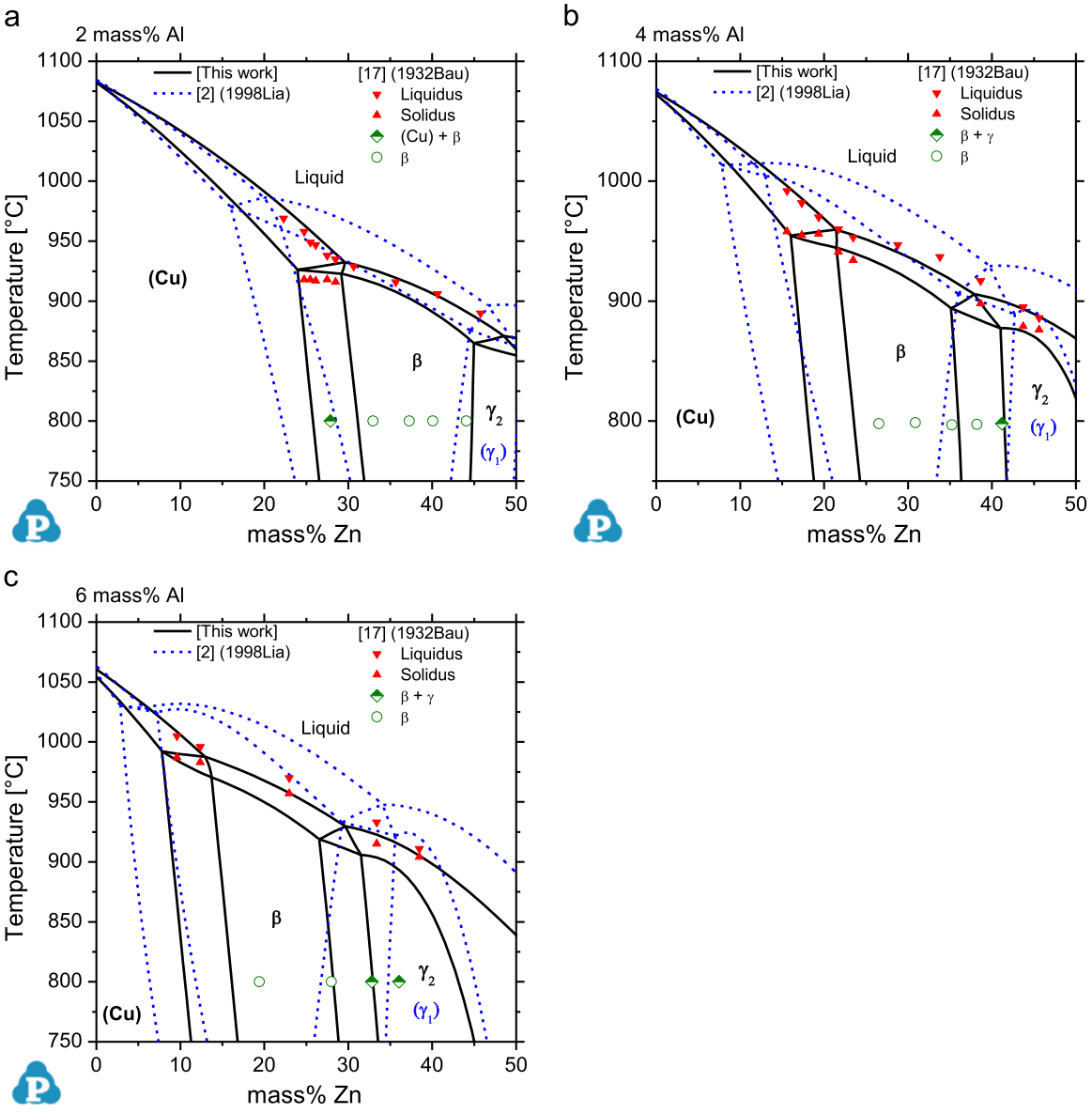

Fig. 12. Comparison of the calculated ternary vertical sections at constant Al content with those calculated with dataset from [2] and experimental data [17]: (a) 2 mass% Al; (b) 4 mass% Al; (c) 6 mass% Al.

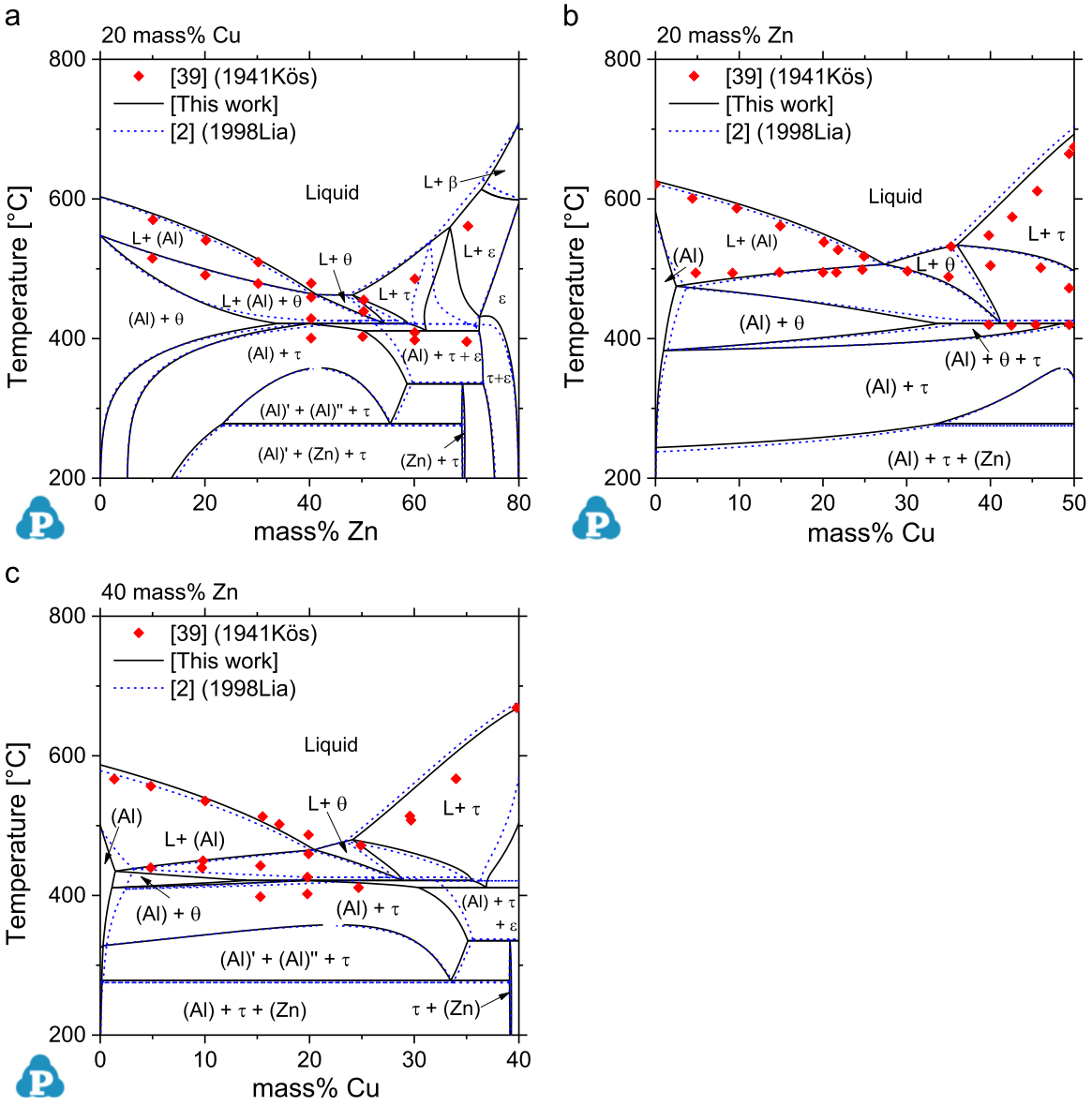

Fig. 13. Comparison of the calculated ternary vertical sections at constant Cu or Zn content with those calculated with dataset from [2] and experimental data [39]: (a) 20 mass% Cu; (b) 20 mass% Zn; (c) 40 mass% Zn.

1150 °C (b). A deviation is noted between the calculated data of the Cu–Zn binary liquid and the experimental data from [41]. However, for the Cu–Zn binary system, there are many other experimental data for the chemical potential and/or activity of Zn in liquid phase. These are comprehensively compared in our previous work on the Cu–Zn binary system, which is the part I of this series, as shown in Fig. 5 of [5].

5. Conclusion

A comprehensive thermodynamic reassessment of the Al–Cu–Zn system is elaborated covering the complete ternary composition range. Partial assessments focusing on the Cu-rich corner only [3,4] cannot be compared to this. Compared to the benchmark full assessment by Liang and Chang [2] the following key progress is emphasized.

1. Significantly revised aspects elaborated in the reassessment of the Al–Cu and Cu–Zn binary systems from Parts I and II of this series are incorporated as basis of the ternary system.
2. The thermodynamic modeling the γ phases is based on a detailed discussion of the crystal structure and simplified only to an extent necessary for a viable application in the ternary system.
3. The experimental data on the γ phases are reexamined, revealing that the γ-CuZn phase connects with the high-temperature Al–Cu phase of same crystal structure in a complete single-phase ternary solid solution range of this disordered γ_2 phase. In contrast, the γ-CuZn phase was connected with the low-temperature Al–Cu phase of different crystal structure in previous work [2].
4. A comprehensive comparison of all presently available experimental phase equilibrium and thermodynamic data with the calculated results is given, enabling a judgment of the present thermodynamic description.

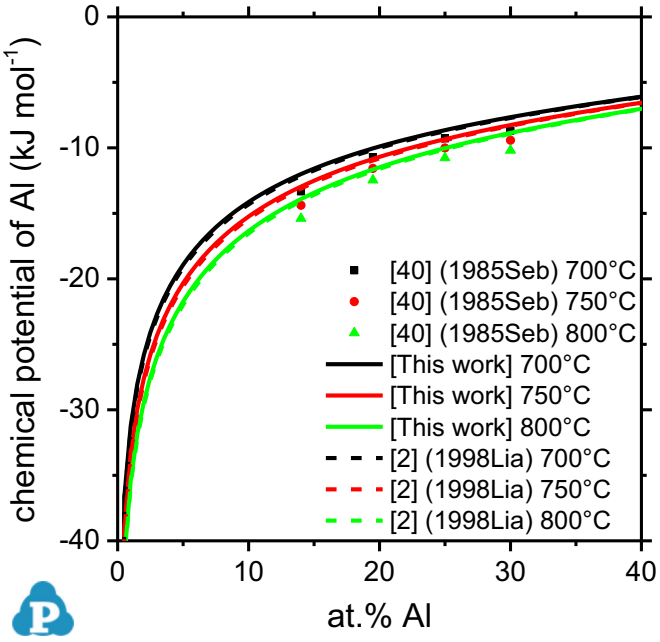

Fig. 14. Comparison of chemical potential of Al in liquid Al–Cu–Zn alloys at constant 7.5 at% Cu calculated in this work with experimental data [40] and calculated results from [2]. Reference state: liquid Al.

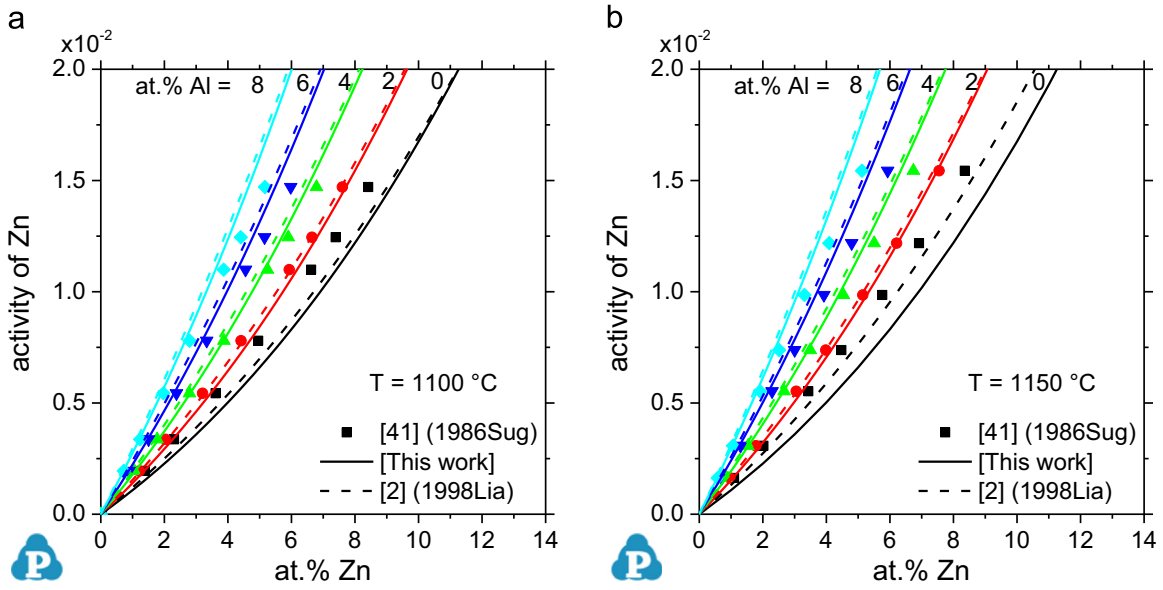

Fig. 15. Comparison of activity of Zn in liquid Cu-rich Al–Cu–Zn alloys and various constant Al-content calculated in this work with experimental data [41] and calculated results from [2] at: (a) 1100 °C; (b) 1150 °C. Reference state: liquid Zn.

Acknowledgment

This study is supported by the German Research Foundation (DFG) under Grant no. Schm 588/41. We acknowledge fruitful discussions with Dr. Jean-Marc Joubert on the structure of the γ phases. We also thank Dr. Svitlana Iljenko for getting the original papers of [15,16] and Dr. Artem Kozlov for careful translation of these papers from Russian.

Appendix A. Supplementary material

Supplementary data associated with this article can be found in the online version at doi:http://dx.doi.org/10.1016/j.calphad.2015.11.001.

References

[1] A.A. Luo, Material design and development: from classical thermodynamics to CALPHAD ICME approaches, Calphad 50 (2015) 6–22.
[2] H. Liang, Y.A. Chang, A thermodynamic description for the Al–Cu–Zn System, J. Phase Equilib. 19 (1998) 25–37.
[3] U. Borggren, M. Selleby, A thermodynamic database for special brass, J. Phase Equilib. 24 (2003) 110–121.
[4] J. Miettinen, Thermodynamic description of the Cu–Al–Zn and Cu–Sn–Zn systems in the copper-rich corner, Calphad 26 (2002) 119–139.
[5] S.-M. Liang, H.-M. Hsiao, R. Schmid-Fetzer, Thermodynamic assessment of the Al–Cu–Zn system, Part I: Cu–Zn binary system, Calphad 51 (2015) 224–232.
[6] S.-M. Liang, R. Schmid-Fetzer, Thermodynamic assessment of the Al–Cu–Zn system, Part II: Al–Cu binary system, Calphad 51 (2015) 252–260.
[7] G. Ghosh, J. van Humbeeck, P. Perrot, Al–Cu–Zn ternary phase diagram evaluation, in: G. Effenberg (Ed.), Ternary Evaluations, MSI, Materials Science International Services GmbH, Stuttgart, 2004.
[8] R. Asahi, H. Sato, T. Takeuchi, U. Mizutani, Verification of Hume-Rothery

electron concentration rule in Cu_5Zn_8 and Cu_9Al_4 γ brasses by ab initio FLAPW band calculations, Phys. Rev. B: Condens. Matter 71 (2005) 165103.
[9] U. Mizutani, T. Noritake, T. Ohsuna, T. Takeuchi, Hume-Rothery electron concentration rule across a whole solid solution range in a series of gamma-brasses in Cu–Zn, Cu–Cd, Cu–Al, Cu–Ga, Ni–Zn and Co–Zn alloy systems, Philos. Mag. 90 (2010) 1985–2008.
[10] S.M. Hao, X.J. Hao, Y.X. Li, Y.P. Ren, H.X. Li, G. Zhao, The compound T′ and the equilibrium phase relationship in low Cu side of Al–Zn–Cu system, Acta Met. Sin. 38 (2002) 694–698.
[11] H. Chen, Y.P. Ren, X. Xin, S.M. Hao, Boundary trend of $\alpha_1/(\alpha_1+\alpha_2)$ phase region at lower Cu side in Al–Zn–Cu system, Trans. Nonferrous Met. Soc. China 14 (2004) 556–559.
[12] H. Chen, X. Xin, D.Y. Dong, Y.P. Ren, S.M. Hao, Study on the stability of T′ phase in the Al–Zn–Cu ternary system, Acta Met. Sin. (Engl. Lett.) 17 (2004) 269–273.
[13] Y.P. Ren, H. Chen, K. Wang, S.M. Hao, D.J. Dong, Effect of Cu addition on the α1+α2 miscibility gap of the Al–Zn system, Scr. Mater. 51 (2004) 267–270.
[14] Y.P. Ren, G.W. Qin, W.L. Pei, S.M. Hao, The $(\alpha_1+\alpha_2)$ miscibility gap of the Al–Zn–Cu system at 360 °C, Scr. Mater. 61 (2009) 36–39.
[15] Z.A. Ashirimbetov, N.E. Kandaurov, M.M. Kalina, V.D. Melikhov, A. A. Presnyakov, Structure and properties of solid solutions of the γ-region of the Cu-Al-Zn system, Prikl. Teor. Fiz. 5 (1973) 210–213.
[16] N.E. Kandaurov, T.B. Begimov, A.A. Presnyakov, V.D. Melikhov, Z. A. Ashirimbetov, Structure of alloys in the γ-region of the copper-aluminum–zinc system at room temperature, Prikl. Teor. Fiz. 3 (1972) 269–275.
[17] O. Bauer, M. Hansen, Der einfluß von-dritten metallen auf die konstitution der messinglegierungen IV. Der einfluß von aluminium, Z. Met. 24 (1932) 73–78.
[18] W. Köster, K. Moeller, Über den aufbau und die volumenänderungen der zink-kupfer-aluminium legierungen I. die aufteilung der konzentrationsebene bei 350°, Z. Met. 33 (1941) 278–283.
[19] N. Ponweiser, C.L. Lengauer, K.W. Richter, Re-investigation of phase equilibria in the system Al–Cu and structural analysis of the high-temperature phase η_1-$Al_{1-\delta}Cu$, Intermetallics 19 (2011) 1737–1746.
[20] L.D. Gulay, B. Harbrecht, The crystal structure of ζ_2-$Al_3Cu_{4-\delta}$, Z. Anorg. Allg. Chem. 629 (2003) 463–466.
[21] L.D. Gulay, B. Harbrecht, The crystal structure of ζ_1-Al_3Cu_4, J. Alloy. Compd. 367 (2004) 103–108.
[22] E.H. Kisi, J.D. Browne, Ordering and structural vacancies in non-stoichiometric Cu-Al γ-brasses, Acta Crystallogr. Sect. B 47 (1991) 835–843.
[23] H.H. Arndt, K. Moeller, Die ternäre phase im system kupfer-aluminium-zink: I. Der zerfall der T-phase zwischen 200 und 300°, Z. Met. 51 (1960) 596–600.
[24] H.H. Arndt, K. Moeller, Die ternäre phase im system kupfer-aluminium-zink: II. Das zustandsgebiet der T-Phase oberhalb 500°, Z. Met. 51 (1960) 656–662.
[25] S. Murphy, The structure of the T′ phase in the system Al–Cu–Zn, Met. Sci. 9 (1975) 163–168.
[26] H.J. Dorantes-Rosales, V.C.M. López-Hirata, J.L. Méndez-Velázquez, M. L. Saucedo-Muñoz, D. Hernández-Silva, Microstructure characterization of phase transformations in a Zn–22 wt%Al–2 wt%Cu alloy by XRD, SEM, TEM and FIM, J. Alloy. Compd. 313 (2000) 154–160.
[27] S.A. Mey, Reevaluation of the Al–Zn system, Z. Met. 84 (1993) 451–455.
[28] S. Kogo, S. Hirosawa, Thermodynamic assessment and determination of spinodal lines for Al–Zn binary system, Mater. Sci. Forum 794–796 (2014) 634–639.
[29] O. von Heidenstam, A. Johansson, S. Westman, A redetermination of the distribution of atoms in Cu_5Zn_8, Cu_5Cd_8, and Cu_9Al_4, Acta Chem. Scand. 22 (1968) 653–661.
[30] O. Gourdon, D. Gout, D.J. Williams, T. Proffen, S. Hobbs, G.J. Miller, Atomic distributions in the γ-brass structure of the Cu – Zn system: a structural and theoretical study, Inorg. Chem. 46 (2007) 251–260.
[31] X.J. Liu, I. Ohnuma, R. Kainuma, K. Ishida, Phase equilibria in the Cu-rich portion of the Cu–Al binary system, J. Alloy. Compd. 264 (1998) 201–208.
[32] S.G. Fries, I. Hurtado, T. Jantzen, P.J. Spencer, K.C. Hari Kumar, F. Aldinger, P. Liang, H.L. Lukas, H.J. Seifert, Present achievements, problems and perspectives associated with a semi-empirical study of the Al–Cu–Mg–Si–Zn light alloy system, J. Alloy. Compd. 267 (1998) 90–99.
[33] I. Ansara, B. Burton, Q. Chen, M. Hillert, A. Fernandez-Guillermet, S.G. Fries, H. L. Lukas, H.-J. Seifert, W.A. Oates, Group 2: models for composition dependence, Calphad 24 (2000) 19–40.
[34] J. Gröbner, Al–Cu binary phase diagram evaluation, in: G. Effenberg (Ed.), Binary Evaluations, MSI, Materials Science International Services GmbH, Stuttgart, 2004.
[35] N. Saunders, System Al–Cu, in: I. Ansara, A.T. Dinsdale, M.H. Rand (Eds.), COST 507: Thermochemical Database For Light Metal Alloys Volume 2: Definition of Thermodynamical and Thermophysical Properties to Provide a Database for the Development of new Light Alloys European Commission, 1998, pp. 28–33.
[36] W. Cao, S.L. Chen, F. Zhang, K. Wu, Y. Yang, Y.A. Chang, R. Schmid-Fetzer, W. A. Oates, PANDAT software with PanEngine, PanOptimizer and PanPrecipitation for multi-component phase diagram calculation and materials property simulation, Calphad 33 (2009) 328–342.
[37] M. Kowalski, P.J. Spencer, Thermodynamic reevaluation of the Cu–Zn system, J. Phase Equilib. 14 (1993) 432–438.
[38] S.L. Chen, S. Daniel, F. Zhang, Y.A. Chang, W.A. Oates, R. Schmid-Fetzer, On the calculation of multicomponent stable phase diagrams, J. Phase Equilib. 22 (2001) 373–378.
[39] W. Köster, Über den aufbau und die volumenänderungen der zink-kupfer-aluminium legierungen, III. Übersicht über den gleichgewichtsverlauf im system kupfer-aluminium-zink, Z. Met. 33 (1941) 289–296.
[40] J. Sebkova, L. Kubicek, Thermodynamic properties of a liquid zinc–aluminum–copper alloy, Kov. Mater. 23 (1985) 3–10.
[41] S. Sugino, H. Hagiwara, Effects of aluminum and nickel on the activity of zinc in molten copper, J. Jpn. Inst. Met. 50 (1986) 1068–1074.